Research on Chemical Intermediates
https://doi.org/10.1007/s11164-019-03744-0

Photocatalytic degradation of benzothiophene by a novel photocatalyst, removal of decomposition fragments by MCM-41 sorbent

Asma Hosseini[1] · **Hossein Faghihian**[1]

Received: 27 October 2018 / Accepted: 12 January 2019

Abstract
In this study, a catalyst was synthesized by introduction of ZnO onto the surface of FSM-16 catalyst support (ZnO/FSM-16). Impregnation of catalyst support by ZnO proceeded through reacting of FSM-16 nanoparticles with $Zn(CH_3COO)_2$ solution followed by calcination of the product. The synthesized photocatalyst was then identified by different methods, and the optical property of the photocatalyst was studied by the DRS method. The results showed that after deposition of photocatalyst on FSM-16 support, the photocatalyst band gap was shifted to the visible region. The photoluminescence studies revealed lower recombination of electron–holes of the photocatalyst after immobilization on FSM-16. The influence of different variables on the photocatalytic performance of the samples was studied. Under optimized conditions, the high degradation efficiency of 97% was obtained by ZnO/FSM-16. The compounds produced from degradation of benzothiophene were recognized by the GC–MS method, and the products containing sulfur were properly adsorbed by MCM-41 sorbent. The photocatalyst showed high regeneration capability, and its activity was mostly preserved after six regeneration cycles.

Keywords Benzothiophene · Zinc oxide · FSM-16 · Degradation products · Adsorption

Introduction

Elimination of pollutants from waste streams by the photooxidation process is considered as an immense development for environmental remediation [1]. Sulfur containing organic compounds are a major pollutant of the crude oil. The hydrodesulfurization process (HDS) is the most conventional method for removal of sulfur compound from

✉ Hossein Faghihian
faghihian@iaush.ac.ir

[1] Department of Chemistry, Shahreza Branch, Islamic Azad University, Shahreza, Iran

Published online: 19 January 2019

transportation fuels. However, this method is not very efficient for removal of benzothiophene and its derivatives. The technique is neither appropriate for profound desulfurization of diesel, since it needs hard operation conditions, hydrogen consumption, and high energy [2]. One of the major organic pollutants of the oil is benzothiophene, which is extremely hard to be eliminated by the conventional desulfurization method.

The photooxidation method is one of the most effective procedures for degradation of organic pollutants. In this method, the hydroxyl radicals generated by UV or visible light irradiation in the presence of an adequate photocatalyst, decompose the organic pollutants to lesser fragments and lastly to carbon dioxide and water [3, 4]. Zinc oxide with excitation energy of 60 meV and band gap of 3.37 eV has been widely used in photodegradation experiments [5, 6]. It is considered as a cost-effective, nontoxic and stable compound compared to other metal oxides [7]. The greatest advantage of ZnO in comparison with TiO_2 is that it is capable of absorbing a higher fraction of UV spectrum resulting in higher degradation efficiency [8, 9]. Immobilization of semiconductor photocatalysts on the surface of adequate supports substantially improve their photoreactivity [10]. FSM-16 material with specific surface are greater than 1000 $m^2\ g^{-1}$, and one-dimensional, and cylindrical-pores with uniform mesoporous size is a desirable candidate for catalyst support [11, 12].

In the present research, we studied the photocatalytic degradation of benzothiophene by use of zinc oxide immobilized on the surface FSM-16. The degradation product were identified by GC-Mass technique and eventually removed via the adsorptive process by use MCM-41 adsorbent.

Experiments

Chemicals and instruments

The chemical reagents including; SiO_2, HNO_3, C_2H_5OH, $HClO_4$, HCl, NaOH, $Zn(CH_3COO)_2$, HF, cetyltrimethylammonium bromide, and benzothiophene were purchased from Merck Company (Germany). An AJASC V 670 diffuse reflectance spectrometer was employed to evaluate the changes on the band gap of the samples. To study the extent of e^-/h^+ recombination, a Cary Eclipse (FL0906M003) photoluminescence device was used. The morphology of the samples was studied by a Philips, PW1730 X-ray diffractometer, and the BET N_2 isotherms were prepared by a Micrometric model ASAP2020 device (USA). The quantity of zinc in the samples was determined by a PG AA500 A.A spectrometer. A GC-Mass spectrometer (Agilent GC 6890 N), was employed to measure the fragments produced from decomposition of the pollutant. Benzothiophene content of the degraded solutions was measured by a Perkin Elmer model Lambda 25 spectrophotometer.

Preparation of photocatalysts

FSM-16 support

FSM-16 Support was synthesized according to the method outlined by A. Matsumoto et al. [13]. Thus, 6.0 g of sodium silicate was added to 120 mL of NaOH solution (0.27 M). The mixture was shaken for 3 h at 25 °C, and was filtered to remove the solid product. It was vacuum dried, and then heat treated at 750 °C for 6 h. Then 3.0 g of heat treated sample was added to 30 mL of distilled water, vigorously shaken for 3 h and then filtered. The pasty material obtained from this step was dispersed into 112 mL of cetyl trimethyl ammonium bromide solution (0.125 M). By adding diluted NaOH, the pH of the mixture was increased to 8.5, and was agitated for 4 h at 65 °C. The product was separated, rinsed with distilled water, and heat treated at 550 °C.

Immobilization of zinc oxide catalyst support

To embed ZnO on the surface of catalyst support, 3.0 g of support was added into 20 mL $Zn(CH_3COO)_2$(0.08 mol L^{-1} in water/ethanol mixture), and agitated for 18 h at 25 °C. The photocatalyst was then removed, and rinsed with ethanol to eliminate the remaining zinc, and dried for 2 h at 95 °C and then calcined at 400 °C for 4 h [14]. According to its zinc oxide content, the photocatalysts were represented as ZnO/FSM-16 (3X %), where X represent the percentage of loaded zinc oxide.

To measure the zinc content of the photocatalysts, 100 mg of the sample was added into a solution containing 5.0 mL of HNO_3 (65 w/v%), 1.0 mL of $HClO_4$ (60 w/v%). The mixture was then gently heat-treated to dryness, and after adding 2.0 mL of HF (30 w/v%), and 10.0 mL of HCl (10 v/v%) was again heated for 25 min. The remaining solid was separated by filtration and the filtrate was diluted to 25 mL with deionized water. The zinc content of the solution was determined.

Degradation of benzothiophene

Degradation of benzothiophene by synthesized catalysts was studied under UV and visible light. To prepare the degradation solution, a predetermined amount of the sample (0.05–0.4 g) was transferred into a degradation cell, and 10 mL of the pollutant solutions (100–600 mg L^{-1}) was added. The mixture was thoroughly shaken until a homogenous suspension was obtained, and then gently shaken in the dark to maintain the adsorption/desorption process at equilibrium. The mixture was put under UV or visible light for a predetermined time (0.0–500 min). As UV source, a 30 W, Philips Hg lamp, and, for visible light, a 30 W fluorescence lamp were used. The lamps were installed 10 cm above the cell [15, 16]. After irradiation, the photocatalyst was removed and the benzothiophene content was measured at $\lambda_{max}=246$ nm. Blank samples (without photocatalysts) were used to evaluate the rate of photolysis of the pollutants. The degradation efficiency was determined by Eq. (1):

$$\%\ \text{Degradation} = \left(\left(A_0 - A_t\right)/A_0\right) \times 100 \tag{1}$$

A_0 and A_t are the absorbance of pollutant before and after irradiation, respectively. The effect of different influencing variables including ZnO content of the photocatalyst, irradiation time, pollutant initial concentration, catalyst dose, and the effect of H_2O_2 on pollutant decomposition was studied.

Discussion of the results

Identification of samples

In FSM-16 pattern four lines belonged to 100, 110, 200, and 210 planes, which are the specific lines of the reference sample, were observed [17] (Fig. 1a) The ZnO pattern comprised of some lines in the 2θ range of 30°–65° which were in good agreement with the hexagonal structure of reference zinc oxide (JCPDS 36-1451) [18]. In the (ZnO/FSM-16(20%)) XRD pattern, all lines belonged to FSM-16, and ZnO without any significant changes of their locations observed, indicating that the structure of catalyst and support was unchanged during the immobilization process. The particle size of the catalysts was estimated by Scherrer's equation;

$$D = 0.9\lambda/\beta \cos\theta. \tag{2}$$

λ is the wavelength of the X-ray, and β is the width of the half maximum line intensity. The particle size of the support, and photocatalyst were, respectively 21, and 49 nm showing that photocatalysts belonged to the nano-sized family of the materials.

The porosity performance of samples including surface area (*S*BET), pore volume (*V*p), and pore are given in Table 1. The adsorption–desorption isotherms

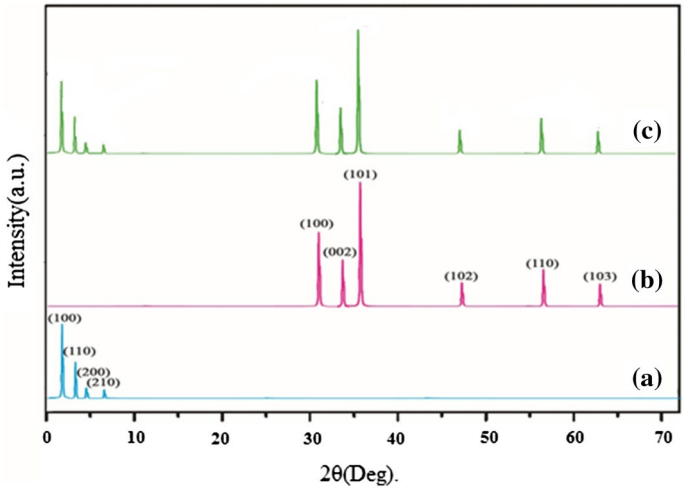

Fig. 1 XRD patterns of FSM-16 (a), ZnO (b), and ZnO/FSM-16 (20%) (c)

Table 1 Specific surface area, pore diameter and pore volume of the photocatalysts

Samples	Specific surface area (m^2/g)	Average pore diameter (nm)	Total pore volume (cm^3/g)
FSM-16	1001.44	4.83	1.21
ZnO/FSM-16	823.14	4.52	0.93

almost coincided in both samples, which was the indication of high mesoporous uniformity of the photocatalysts (Fig. 2) [19]. Owing to the occupation of the FSM-16 pores by ZnO molecules, the porosity of ZnO/FSM-16 was slightly lower than FSM-16. However, the synthesized catalyst had the surface of 834.14 m^2 g^{-1} which was bigger that of the previously reported samples [20]. Mehrabadi et al. prepared TiO_2/

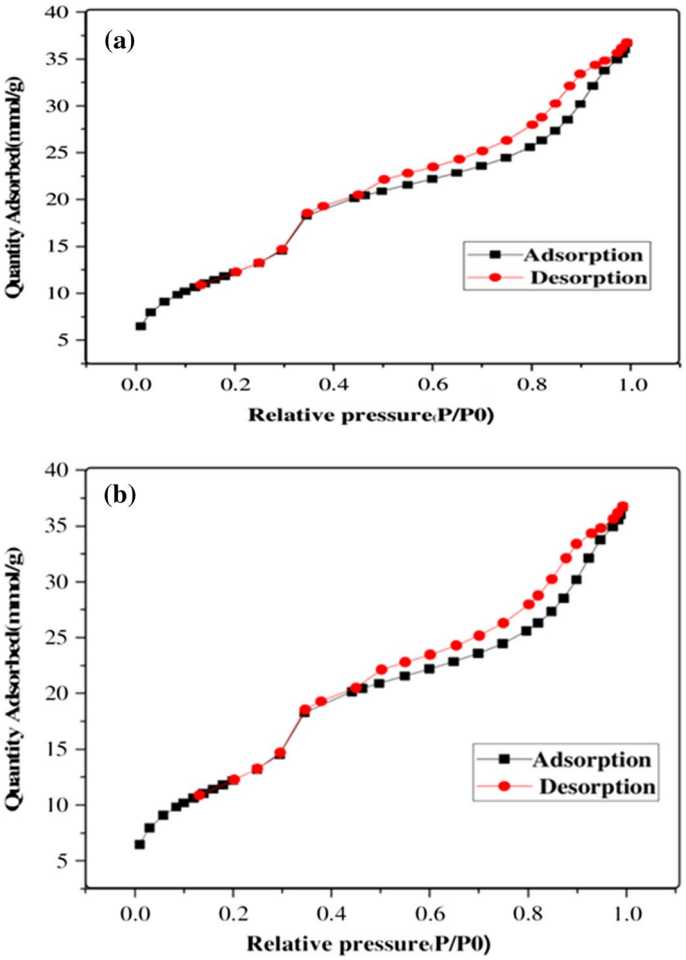

Fig. 2 Nitrogen adsorption–desorption isotherms of FSM-16 (**a**) and ZnO/FSM-16 (**b**)

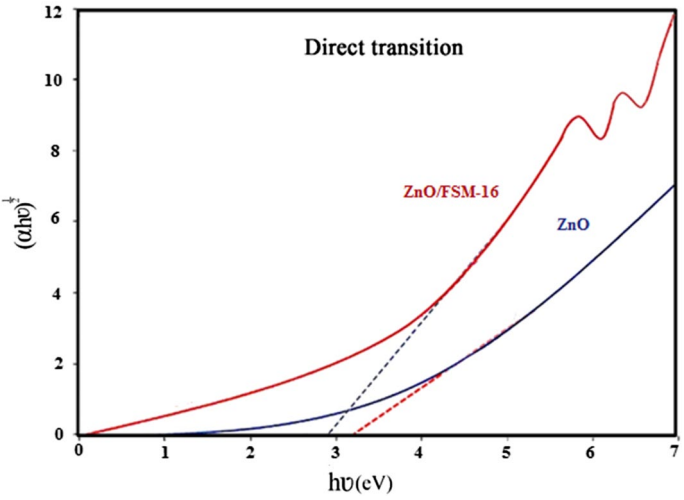

Fig. 3 DRS spectra of ZnO, and ZnO/FSM-16 samples

Table 2 Direct bandgaps of the photocatalysts (eV)

	Photocatalysts	
n	ZnO	ZnO/FSM-16
1/2	3.37	2.91

NCP photocatalyst by deposition of TiO_2 on NCP support and reported that the low specific area of 51.46 $m^2\ g^{-1}$ [3].

Optical property of ZnO and ZnO/FSM-16

DRS spectra

The DRS spectra were taken by use of $BaSO_4$ as the reference compounds, and were analyzed by the Kubelka–Munk and Tauc plots. The photocatalyst band gap was determined through Eqs. (3, 4) [21, 22].

$$K = (1 - R)^2/2R \tag{3}$$

K is the transformed reflectance, and R is the percentage of reflected light (%) [23]. By plotting of $(\alpha h\nu)^{1/2}$ versus $h\nu$ through Tauc equations, the photocatalysts band gaps were calculated (Fig. 3) [24]:

$$\alpha h\nu = k\left(h\nu - E_g\right)^n \tag{4}$$

υ is photofrequency, h is Planck's constant, and α is the absorption coefficient.

The results showed after introduction of ZnO on to the support, a considerable shift on band gap was observed (Table 2). The shift was from 3.37 to 2.91 eV. The

significant shift was very advantageous for using the ZnO/FSM-16 photocatalyst for degradation of benzothiophene by visible light irradiation [25].

Photoluminescence analysis

To determine the extent of electron–hole recombination, the photoluminescence spectra of the photocatalysts were prepared by excitation of the sample at 290 nm. The emission peaks appeared at 377 and 420 nm for ZnO and at 377, 420, and 480 nm for ZnO/FSM-16 (Fig. 4). After introduction of zinc oxide, the peaks belonging to ZnO appeared with lower intensity indicating that the process decreased the recombination of e^{-}/h^{+}. The lower electron–hole recombination of ZnO/FSM-16 increased its catalytic efficacy for degradation of benzothiophene. On the other hand, the lower band gap of ZnO/FSM-16 confirmed by the DRS spectra, facilitated the decomposition of benzothiophene by visible light irradiation. From this data it was concluded that the synthesized ZnO/FSM-16 photocatalyst had considerable capability for degradation of the studied pollutant under visible light irradiation. Mehrabadi et al. who immobilized TiO_2 on clinoptilolite for degradation of atenolol reported a similar effect [3]. Habibi–Yongjeh studied the photoluminescence of nanocomposites prepared by incorporation of g-C_3N_4 into Ag_2SO_4 and Fe_3O_4/AgI/Ag_2CrO_4, and reported that the photoluminescence intensity of g-C_3N_4 was significantly decreased [26].

Optimizing of photocatalysts efficiency

Effect of catalyst support

To evaluate the influence of FSM-16 support on the degradation yield of benzothiophene, decomposition of benzothiophene was studied by ZnO (bulk), and zinc oxide

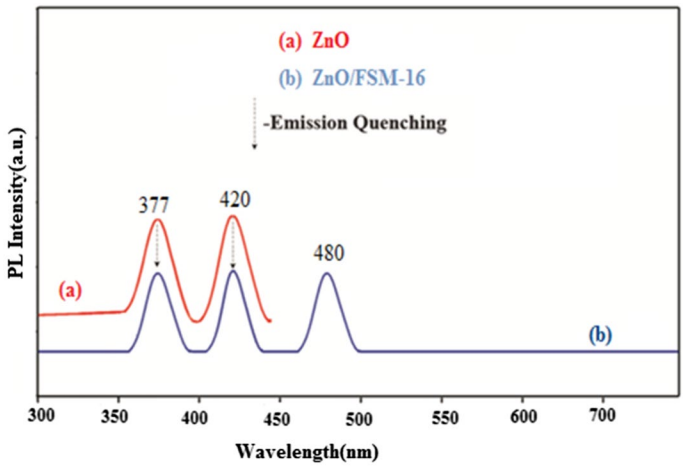

Fig. 4 PL spectra of ZnO (a), ZnO/FSM-16 (b)

immobilized on the support. Photolysis, and dark adsorption of benzothiophene was also measured (Fig. 5). The results indicated that the photolysis of benzothiophene was insignificant, and the degradation yield obtained by FSM-16 was also very limited. The degradation efficiency of benzothiophene by bulk ZnO was, respectively, 53 and 40% by UV and visible light. However, ZnO/FSM-16 had higher activity than bulk ZnO. The higher activity of ZnO/FSM-16 was in agreement with the results obtained by photoluminescence analysis. The PL analysis showed that recombination of e^{-}/h^{+} was much lower in ZnO/FSM-16. In addition, the catalyst support facilitate the homogenous adsorption of the pollutant by the photocatalyst which in turn enhanced the effective interactions between benzothiophene molecules and generated radicals on the surface of the catalyst [25]. Derikvandi et al., who used NiO and ZnO immobilized on clinoptilolite support for decomposition of metronidazole reported, that the degradation efficiency of photocatalyst immobilized on the surface of the support was much higher that the value obtained by

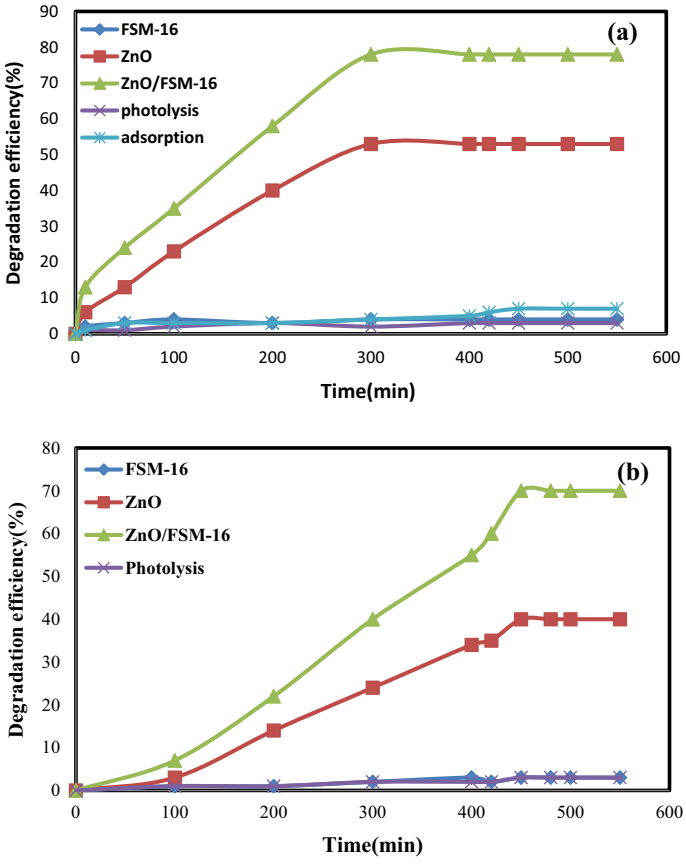

Fig. 5 Degradation of benzothiophene versus times under UV (**a**) and visible light (**b**) irradiations (catalyst dose = 0.1 g L^{-1}, benzothiophene concentration = 100 mg L^{-1}, irradiation time = 450 min, and temperature = 25 °C)

bulk samples [27]. Bahrami et al. investigated the influence of deposition of FeO and ZnO on clinoptilolite nano-particles and reported higher degradation after the immobilization process [28]. Mirian et al. evaluated phenol degradation by heterogeneous photodegradation process in the presence of FeO immobilized onto clinoptilolite and reported a significant improvement on the degradation efficiency after loading of the photocatalyst on the support surface [29].

Irradiation time

The performance of photocatalyst for decomposition of benzothiophene was evaluated between 0 and 550 min. The mixture containing 0.2 g of ZnO/FSM-16 in 25 mL of benzothiophene solution (100 mg L^{-1}) was agitated for a predetermined time while UV or visible light was used for irradiation. The catalyst was removed by filtration, and benzothiophene concentration was determined (Fig. 5). By increase of irradiation time, decomposition of benzothiophene was increased and achieved a maximum within 300 min. The time needed for equilibration was smaller than many studied photocatalysts. For example, decomposition of the benzothiophene and dibenzothiophene in the presence of ZnO, and TiO_2 respectively needed 420, and 600 min for equilibrium [20, 30].

Catalyst dose

The capability of the photocatalyts was examined with different doses (0.05–0.4 g L^{-1}) (Fig. 6). By increasing of photocatalyst concentration, the degradation of benzothiophene was initially increased and then remained constant, and the optimized photocatalyst concentration of 0.3 g L^{-1} was obtained. By increasing catalyst dose, more active centers were available to receive the incident photons and to produce more electron/hole pairs. Beyond the optimized value, the aggregation of nanoparticles reduced their surface area, and the incident photons are partially scattered [30, 31]. The optimal dose of each particular photocatalyst depends on several variables such as; particle size, pore volume and its surface charge. Ajoudanian et al. employed natural zeolite, clinoptilolite coupled with NiO for decomposition of cephalexin. The results indicated that the optimal extent of decomposition was achieved by 0.2 g L^{-1} of the catalyst [32]. Nezamzadeh–Ejhieh employed a catalyst prepared by immobilization of CuO on clinoptilolite support for p-aminophenol degradation. The maximal degradation efficiency was obtained with 2.0 g L^{-1} of the photocatalyst [33]. Clinoptilolite embedded with ZnO was used for photodecomposition of phenylhydrazine, and the maximal decomposition was achieved with 0.25 g L^{-1} of catalyst [18].

Pollutant concentration

The influence of pollutant concentration on photodegradation efficacy was investigated in solutions containing 100–600 mg L^{-1} (Fig. 7). The maximal efficiency was obtained at a concentration of 200 mg L^{-1}. At very low concentration, the amount of benzothiophene close to the surface of the catalyst was insufficient, and

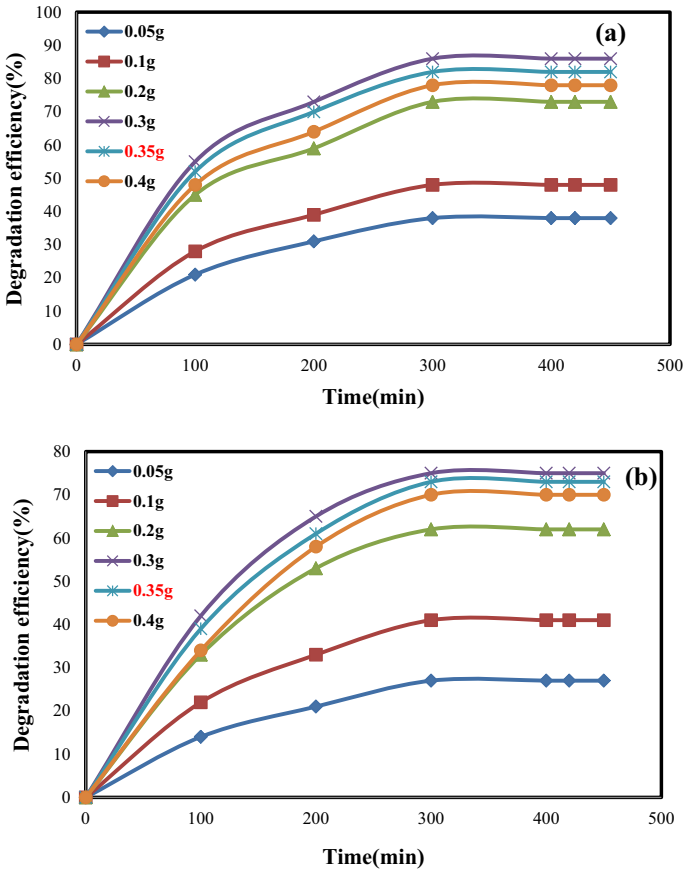

Fig. 6 Effect of catalyst dose on benzothiophene degradation under UV (**a**) and visible light (**b**) irradiations: (benzothiophene concentration = 100 mg L^{-1}, irradiation time = 450 min, ZnO loading = 20%, and temperature = 25 °C)

due to the extremely short lifetime of electron–hole pairs, they are recombined before interaction with pollutant molecules [30, 34]. As the concentration was increased, the rate of migration of benzothiophene from bulk of solution towards photocatalyst was increased. Therefore, the OH radicals generated on the surface reacted more efficiently with the pollutant molecules, and the maximal degradation of 88, and 83% was obtained, respectively, with UV and visible light irradiation at 200 mg L^{-1}. Beyond optimized concentration, the absorption of incident photons by the pollutant molecules led to lower radical generation [30]. The optimized concentration depended on various parameters such as catalyst reactivity, catalyst dose and the nature of the pollutants. Nezamzadeh-Ejhieh et al. employed ZnO supported-nano-clinoptilolite for photodegradation of 4-nitrophenol, and reported the optimized degradation with pollutant concentration of 10 mg L^{-1}

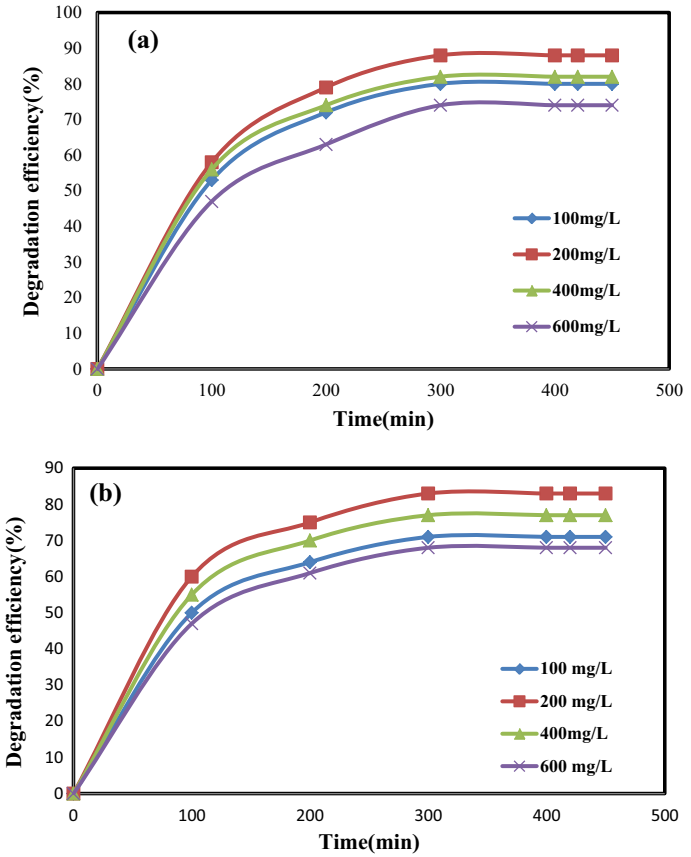

Fig. 7 Effect of initial benzothiophene concentration on degradation efficiency under UV (**a**) and visible light (**b**) irradiations (catalyst dose = 0.1 g L^{-1}, irradiation time = 450 min, ZnO loading = 20%, and temperature = 25 °C)

[35], while the optimized concentration of dibenzothiophene degraded by La/PEG catalyst modified with TiO_2 was 250 mg L^{-1} [36].

ZnO loading

The effect of ZnO loading on the photocatalyst performance was evaluated by use of catalysts with different ZnO loading (3–25%) (Fig. 8). The results showed that the catalyst containing 20% of ZnO had the maximal degradation efficiency, and under an optimized condition (catalyst dose of 0.3 g L^{-1}, benzothiophene concentration of 200 mg L^{-1}, irradiation time of 300 min, and temperature of 25 °C), the high degradation efficiency of 97% was obtained by ZnO/FSM-16. The lower extent of degradation obtained at higher zinc oxide content was due to the particles aggregation, reducing the number of active sites [4, 37]. Similar observation was reported by Li et al. who used Pt-TiO_2 catalyst for photocatalytic oxidation of methylene blue

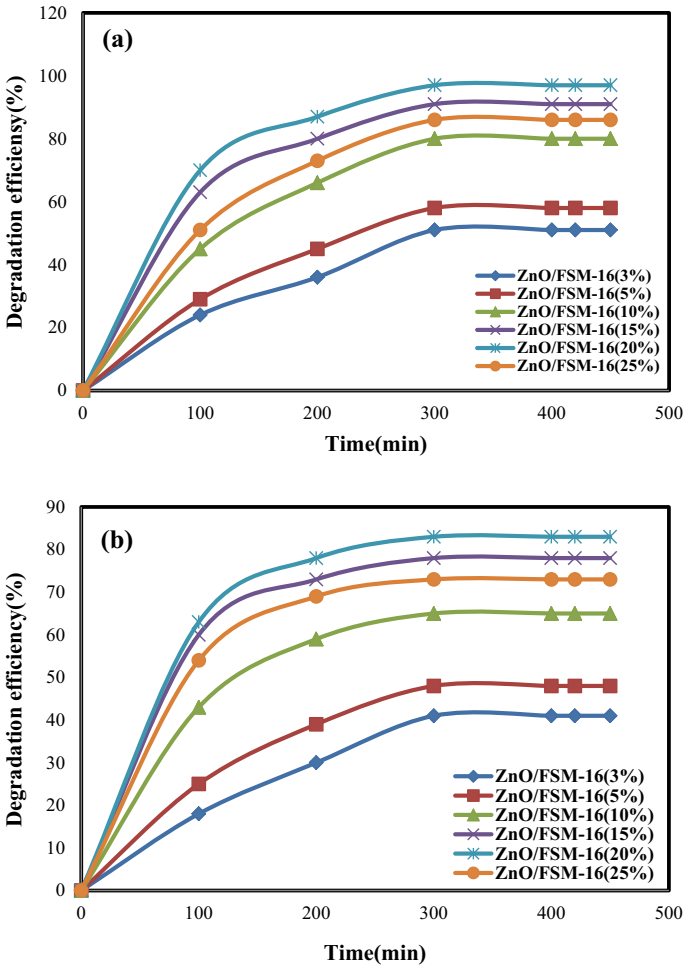

Fig. 8 Effect of ZnO loading on benzothiophene degradation under UV (**a**) and visible light (**b**) irradiations: (benzothiophene concentration = 200 mg L^{-1}, catalyst dose = 0.3 g L^{-1}, irradiation time = 300 min, and temperature = 25 °C)

and methyl orange in aqueous solutions and observed that the optimal efficiency was obtained with a catalyst containing 75% of Pt [38]. Lu et al. used a catalyst prepared by immobilization of zinc oxide on MCM-41 for methyl benzoate hydrogenation and reported that the optimized efficiency was obtained with the photocatalyst containing 10% of ZnO [39].

Addition of H_2O_2

The influence of H_2O_2 on the photodegradation of the benzothiophene was evaluated with various amounts of H_2O_2 added to 10 mL of solution (Fig. 9). By increasing

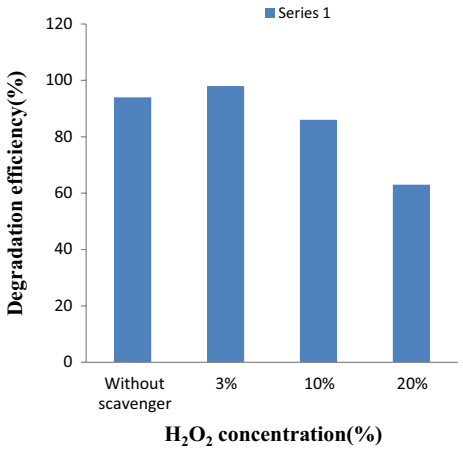

Fig. 9 Effect of H_2O_2 addition on benzothiophene degradation: (benzothiophene concentration = 200 mg L^{-1}, catalyst dose = 0.3 g L^{-1}, irradiation time = 300 min, ZnO content: 20%, and temperature = 25 °C)

hydrogen peroxide concentration, the photodegaradtion extent was enhanced, and the maximal extent was obtained at a concentration of 3%. This was attributed to the generation of more $OH^{\cdot}$ radicals according to Eqs. (5) and (6). Beyond the optimized concentration, the degradation was reduced, because the extra amount of H_2O_2 trapped the $OH^{\cdot}$ radicals to form weaker $HO_2^{\cdot}$ radicals which again reacted to $OH^{\cdot}$ radicals to form H_2O (Eqs. 7, 8) [36].

$$e^{-} + H_2O_2 + \rightarrow OH^{\cdot} + OH^{-} \tag{5}$$

$$O_2^{-} + H_2O_2 \rightarrow O_2 + OH^{\cdot} + OH^{-} \tag{6}$$

$$H_2O_2 + OH^{\cdot} \rightarrow H_2O + OH_2^{\cdot} \tag{7}$$

$$HO_2^{\cdot} + OH^{\cdot} \rightarrow H_2O + O_2 \tag{8}$$

The positive influence of H_2O_2 on decomposition of dibenzothiophene by two modified molecular sieves; Ti-MCM-41, and its modified form was reported by Zhang et al. [40]. Dishun studied photocatalytic decomposition of dibenzothiophene by use of TS-1, and reported that optimization of the reaction condition occurred in the presence of 30% of H_2O_2 [41].

Identification and elimination of degradation products

The compounds produced from decomposition of the pollutant were studied by GC–MS technique using an Agilent GC 6890 N instrument, and He as carrier (Figs. 10, 11). The identified compounds include tridecane, heptadecane, 3-methyl heptadecane, cyclohexane, 1,1-dimethyl, 2-pentyl thiophene and thiophene and are respectively given in Tables 3 and 4, and the corresponding chromatograms are respectively represented in Figs. 10 and 11. Among them, 1-dimethyl, 2-pentyl thiophene and thiophene are sulfur containing products which were removed by

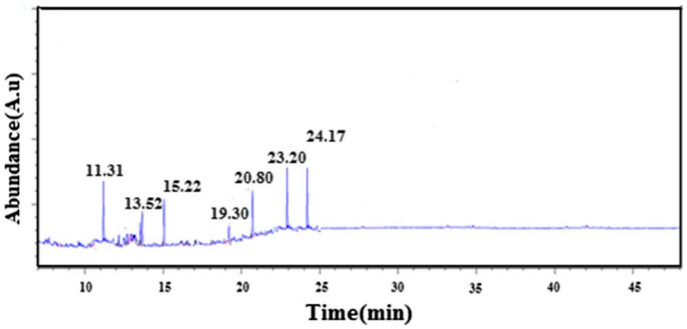

Fig. 10 Identified degradation products produced by UV irradiation before adsorption

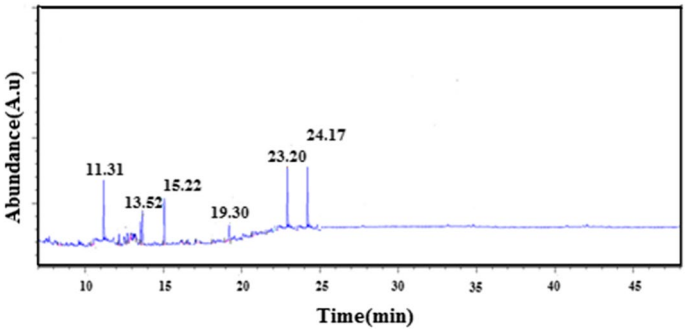

Fig. 11 Identified degradation products produced by visible light irradiation before adsorption

Table 3 Identified degradation products produced by UV irradiation (before adsorption and after adsorption)

Before adsorption		After adsorption	
Products	Retention time (min)	Products	Retention time (min)
Benzothiophene	11.31	Benzothiophene	11.31
Tridecane	13.52	N.d*	
Heptadecane	19.30	N.d*	
3-Methylheptadecane	20.80	3-Methylheptadecane	20.80
Cyclohexane, 1,1-dimethyl	15.22	Cyclohexane, 1,1-dimethyl	15.22
2-Pentyl, thiophene	24.17	N.d*	
Thiophene	23.20	N.d*	

*N.d** not detected

the adsorption method as the complementary section of this research. MCM-41 was employed as the adsorbent material. The procedure was performed through adding 0.2 g of MCM-41 into 50 mL of degradation solution. After shaking for 6 h at

Table 4 Identified degradation products produced by visible light irradiation (before adsorption and after adsorption)

Before adsorption		After adsorption	
Products	Retention time (min)	Products	Retention time (min)
Benzothiophene	11.31	Benzothiophene	11.31
Tridecane	13.52	N.d*	
Heptadecane	19.30	N.d*	
Cyclohexane, 1,1-dimethyl	15.22	Cyclohexane, 1,1-dimethyl	15.22
2-Pentyl, thiophene	24.17	N.d*	
Thiophene	23.20	N.d*	

*N.d** not detected

25 °C, the sorbent was removed by centrifugation, and the remaining compounds in the solution were identified. The corresponding chromatograms are represented in Figs. 12 and 13, respectively, for the UV and visible irradiation, and the identified compounds are listed respectively in Tables 3 and 4. The results indicated that the sulfur containing products; 1-dimethyl, 2-pentyl thiophene and thiophene were properly eliminated. The outcome of this research confirmed that combination of photodegradation-adsorption processes can be considered as it is an efficient technique for removal of benzothiophene which is a typical aromatic organosulfur compound that cannot be removed by HDS technique.

Regeneration of photocatalysts

To develop a cost effective photodegradation procedure, regeneration capability of the photocatalyst must be evaluated. In this work, the used photocatalyst was washed with n-hexane to eliminate the organic materials adhering to the surface of the photocatalyst and shielding the active sites. Then the reaming compounds were eliminated by a heat treatment procedure. To obtain the lowest needed

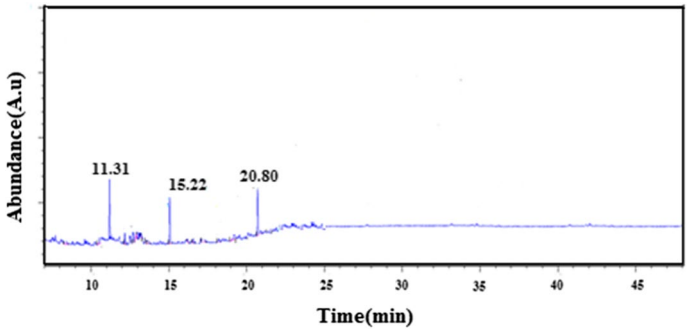

Fig. 12 Identified degradation products produced by UV irradiation after adsorption

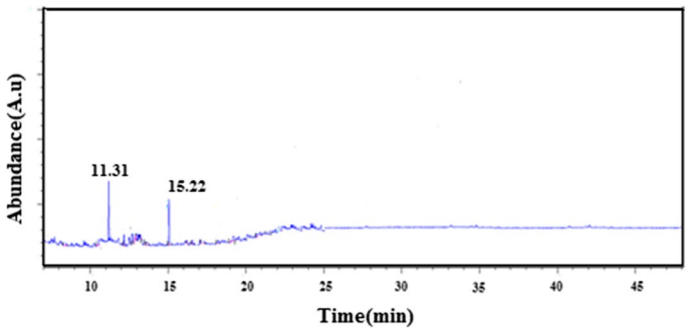

Fig. 13 Identified degradation products produced by visible light irradiation after adsorption

temperature, the treatment was performed at 150, and 450 °C for 3 h. The results indicated that the catalyst treated at 450 °C had more catalytic activity [25, 42]. The efficiency of the regenerated catalysts was then evaluated for six successive regeneration cycles (Fig. 14).

Torki et al. used NiS-PPY-Fe_3O_4 for decomposition of cephalexin and reported that regeneration of the used catalyst could be performed for five cycles [16]. Ajoudanian et al. used nickel oxide supported on clinoptilolite for photodecomposition of cephalexin and concluded that recovery was limited to three cycles. [32].

Kinetics of the process

The kinetics of photodecomposition was studied by a Langmuir–Hinshelwood model. The model can be expressed by Eq. (9):

$$-\ln\ C_t/C_0 = k_p t. \tag{9}$$

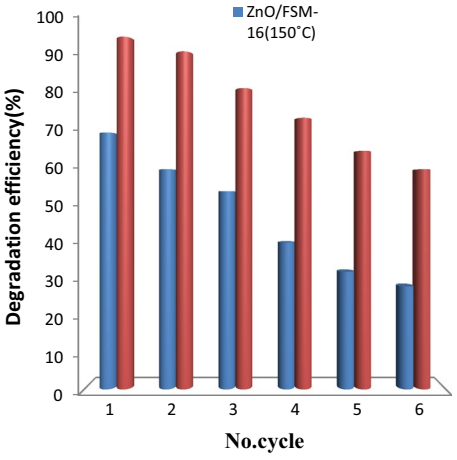

Fig. 14 Regeneration of photocatalyst

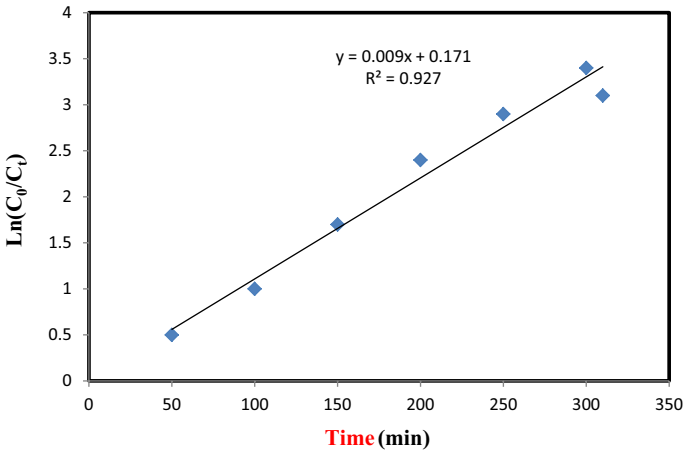

Fig. 15 Pseudo-first-order kinetics for degradation of benzothiophene

C_t and C_0 are, respectively, the quantity of the pollutant at zero and t time (min), and k_p is the rate constant (Fig. 15).

By plotting of $-\ln(C_t/C_0)$ versus t, a straight line with the R^2 value of 0.975 was obtained indicating that the degradation reaction followed first-order kinetics. Dependency of the photodegradation reaction on the concentration of the organic pollutant and description of the data by the Langmuir–Hinshelwood model has already been reported by Qiu et al. They studied the application of PbS–CdS-clinoptilolite catalyst for the catalytic oxidation as a mixture of tetracycline/cephalexin mixture and showed that the reaction followed a first-order kinetic [43].

Conclusions

In this research, a new photocatalyst was prepared by immobilization of Zn onto the structure of FSM-16 mesoporous. The synthesized photocatalysts were then successfully employed for oxidative decomposition of benzothiophene under UV and visible light. From the results of experiments, it was revealed that by deposition of ZnO on the FSM-16, the decomposition rate of the pollutant was significantly enhanced, particularly with visible light irradiation, because, after immobilization, zinc oxide band gap was reduced. The H_2O_2 presence increased photooxidation of the sample. The recovering capability of the catalyst was high, and its degradation performance was mostly retained after six cycles. The compounds produced by degradation of benzothiophene were measured and identified through the GC-Mass method. The sulfur containing degradation products were properly eliminated by the adsorption

method using MCM-41 adsorbent. Therefore, the combined degradation-adsorption method can be considered as an efficient method for elimination of the sulfur-containing compounds of the transportation fuels so that the recent acceptable level of sulfur for the fuel is fulfilled.

References

1. R.M. Mohamed, E.S. Aazam, Clean Soil Air Water **43**, 421 (2015)
2. D. Zhao, F. Li, E. Zhou, Z. Sun, Chem. Res. Chin. Univ. **24**, 96 (2008)
3. Z. Mehrabadi, H. Faghihian, Spectrochim. Acta A. **204**, 248 (2018)
4. A. Nezamzadeh-Ejhieh, M. Karimi-Shamsabadi, Chem. Eng. J. **228**, 631 (2013)
5. C.-Y. Kuo, C.-H. Wu, S.-T. Chen, Desalin. Water Treat. **52**, 834 (2014)
6. U. Koch, A. Fotik, H. Weller, A. Henglein, Chem. Phys. Lett. **122**, 507 (1985)
7. P.R. Westmoreland, D.P. Harrison, Environ. Sci. Technol. **10**, 659 (1976)
8. M.A. Behnajady, N. Modirshahla, R. Hamzavi, J. Hazard. Mater. **133**, 226 (2006)
9. M. Nasser, A.B.M. Ali, B. Oskui, J. Reza, Iran. J. Chem. Chem. Eng. **28**, 49 (2009)
10. B.Y. Jibril, A.Y. Atta, Y.M. Al-Waheibi, T.K. Al-Waheibi, J. Ind. Eng. Chem. **19**, 1800 (2013)
11. D. Shouro, Y. Moria, T. Nakajima, S. Mishima, Appl. Catal. A Gen. **198**, 275 (2000)
12. Y. Tozuka, S. Sasaoka, A. Nagae, K. Moribe, T. Oguchi, K. Yamamoto, J. Colloid Interface Sci. **291**, 471 (2005)
13. A. Matsumoto, T. Sasaki, N. Nishimiya, K. Tsutsumi, Colloids Surf. A. **203**, 185 (2002)
14. Y. Xiong, L.Z. Zhang, G.Q. Tang, G.L. Zhang, W.J. Chen, J. Lumin. **110**, 17 (2004)
15. X. Li, Y. Pi, Q. Xia, Z. Li, J. Xiao, Appl. Catal. B Environ. **41**, 5077 (2016)
16. F. Torki, H. Faghihian, J. Photochem. Photobiol. A Chem. **338**, 49 (2017)
17. S.H. Garg, K. Soni, M. Kumar, T. Bhaskar, J.K. Gupta, K.S. Rama Rao, G. Murali Dhar, Catal. Today **198**, 263 (2012)
18. A.R. Nezamzadeh-Ejhieh, F. Khodabakhshi-Chermahini, Ind. Eng. Chem. Res. **20**, 695 (2014)
19. N. Hazrati, M. Abdouss, A. Vahid, A.A. Miran Beigi, A. Mohammadalizadeh, Int. J. Environ. Sci. Technol. **11**, 997 (2014)
20. A. Hosseini, H. Faghihian, A.M. Sanati, Mater. Sci. Semicond. Process. **87**, 110 (2018)
21. J. Esmaili-Hafshejani, A. Nezamzadeh-Ejhieh, J. Hazard. Mater. **316**, 194 (2016)
22. V. Džimbeg-Malčić, Ž. Barbarić-Mikočević, K. Itrić, Tech. Gaz. **18**, 117 (2011)
23. Z. Mehrabadi, H. Faghihian, J. Photochem. Photobiol. A **356**, 102 (2018)
24. J. Tauc, R. Grigorovici, A. Vancu, Phys. Status Solidi B **15**, 627 (1996)
25. H. Zabihi-Mobarakeh, A. Nezamzadeh-Ejhieh, J. Ind. Eng. Chem. **20**, 1421 (2014)
26. A. Akhundi, A. Habibi-Yangjeh, Adv. Powder Technol. **27**, 2496 (2016)
27. H. Derikvandi, A. Nezamzadeh-Ejhieh, J. Hazard. Mater. **321**, 629 (2017)
28. M. Bahrami, A. Nezamzadeh-Ejhieh, Mater. Sci. Semicond. Process. **27**, 833 (2014)
29. Z.A. Mirian, A. Nezamzadeh-Ejhieh, Desalin. Water Treat. **57**, 16483 (2016)
30. S. Matsuzawa, J. Tanaka, S. Sato, T. Ibusuki, J. Photochem. Photobiol. A **149**, 183 (2002)
31. D. Mijin, J. Radivojevic, P. Jovancic, Chem. Ind. Chem. Eng. Q. **13**, 33 (2007)
32. N. Ajoudanian, A. Nezamzadeh-Ejhieh, Mater. Sci. Semicond. Process. **36**, 162 (2015)
33. A. Nezamzadeh-Ejhieh, M. Amiri, Powder Technol. **235**, 279 (2013)
34. Z. Long, C. Yang, G. Zeng, L. Peng, C. Dai, H. He, Fuel **130**, 19 (2014)
35. A. Nezamzadeh-Ejhieh, S. Khorsandi, Ind. Eng. Chem. Res. **20**, 937 (2014)
36. S. Moradi, M. Vossoughi, M. Feilizadeh, S.M. Esmaeil Zakeri, M.M. Mohammadi, D. Rashtchian, A. Yoosefi Booshehri, Res. Chem. Intermed. **41**, 4151 (2015)
37. Y. Ji, L. Zhou, C. Ferronato, X. Yang, A. Salvador, C. Zeng, J.-M. Chovelon, J. Photochem. Photobiol. A Chem. **254**, 35 (2013)
38. F.B. Li, X.Z. Li, Chemosphere **48**, 1103 (2002)
39. W. Lu, G. Lu, Y. Luo, A. Chen, J. Mol. Catal. A Chem. **188**, 225 (2002)
40. J. Zhang, D. Zhao, Z. Ma, Y. Wang, Catal. Lett. **138**, 111 (2010)
41. Z. Juan, Z. Dishun, Y. Liyan, L. Yongbo, Chem. Eng. J. **156**, 528 (2010)

42. D.H. Tseng, L.C. Juang, H.H. Huang, Int. J. Photoenergy **2012**, 1 (2012)
43. J. Qiu, G. Wang, Y. Zhang, D. Zeng, Y. Chen, Fuel **147**, 195 (2015)